



Published in final edited form as:

*Biol Psychiatry*. 2019 August 01; 86(3): 171–184. doi:10.1016/j.biopsych.2018.08.009.

## RPS23RG1 is Required for Synaptic Integrity and Rescues Alzheimer's Associated Cognitive Deficits

Dongdong Zhao<sup>1</sup>, Jian Meng<sup>1</sup>, Yingjun Zhao<sup>2</sup>, Yuanhui Huo<sup>1</sup>, Yan Liu<sup>2,3</sup>, Naizhen Zheng<sup>1</sup>, Muxian Zhang<sup>1</sup>, Yue Gao<sup>1</sup>, Zhicai Chen<sup>1</sup>, Hao Sun<sup>1</sup>, Xiangyu Wang<sup>4</sup>, Chuya Jing<sup>1</sup>, Tongmei Zhang<sup>2</sup>, Xian Zhang<sup>1</sup>, Hong Luo<sup>1</sup>, Xin Wang<sup>1</sup>, Jie Zhang<sup>1</sup>, Fa-rong Liu<sup>5</sup>, Yanfang Li<sup>1</sup>, Guojun Bu<sup>1,6</sup>, Lei Wen<sup>3</sup>, Timothy Y. Huang<sup>2</sup>, Huaxi Xu<sup>#1,2</sup>, and Yun-wu Zhang<sup>#1</sup>

<sup>1</sup>Fujian Provincial Key Laboratory of Neurodegenerative Disease and Aging Research, Institute of Neuroscience, Medical College of Xiamen University, Xiamen, Fujian 361102, China

<sup>2</sup>Neuroscience Initiative, Sanford-Burnham-Prebys Medical Discovery Institute, La Jolla, CA 92037, USA

<sup>3</sup>Department of Traditional Chinese Medicine, Medical College of Xiamen University, Xiamen, Fujian 361102, China

<sup>4</sup>State Key Laboratory of Molecular Vaccinology and Molecular Diagnostics & Center for Molecular Imaging and Translational Medicine, School of Public Health, Xiamen University, Xiamen 361005, China

<sup>5</sup>Psychology Department, Xiamen Xianyue Hospital, Xiamen, Fujian 361012, China

<sup>6</sup>Department of Neuroscience, Mayo Clinic, Jacksonville, FL 32224, USA

# These authors contributed equally to this work.

### Abstract

**BACKGROUND:** Although synaptic impairment is prerequisite to cognitive deficiencies in Alzheimer's disease (AD), mechanisms underlying the dysregulation of essential synaptic scaffolding components and their integrity remain elusive. RPS23RG1 is a newly identified protein implicated in AD. However, the physiological function of RPS23RG1 has yet to be determined.

**METHODS:** We investigated the role of RPS23RG1 in maintaining synaptic structure and function in cell cultures and in *Rps23rg1* knockout mice, and determined whether targeting RPS23RG1-mediated pathway has therapeutic potential in APP/PS1 AD model mice.

---

**Correspondence to:** Yun-wu Zhang, Fujian Provincial Key Laboratory of Neurodegenerative Disease and Aging Research, Institute of Neuroscience, Medical College of Xiamen University, Xiamen, Fujian 361102, China (yunzhang@xmu.edu.cn; Tel: 86-592-2188528; Fax: 86-592-2188528).

The authors report no biomedical financial interests or potential conflicts of interest.

**Publisher's Disclaimer:** This is a PDF file of an unedited manuscript that has been accepted for publication. As a service to our customers we are providing this early version of the manuscript. The manuscript will undergo copyediting, typesetting, and review of the resulting proof before it is published in its final citable form. Please note that during the production process errors may be discovered which could affect the content, and all legal disclaimers that apply to the journal pertain.

**RESULTS:** Deletion of the *Rps23rg1* gene resulted in severe memory deficits and impairment of post-synaptic structure and function, with marked reductions in PSD-93 and PSD-95 levels. RPS23RG1 interacted with PSD-93/PSD-95 through its intracellular domain, consequently sequestering PSD-93/PSD-95 from MDM2-mediated ubiquitination and degradation, thereby maintaining synaptic function. Restoration of PSD-93/PSD95 levels reversed synaptic and memory deficits in *Rps23rg1* KO mice. We further observed attenuated RPS23RG1 expression in human AD, which positively correlated with PSD-93/PSD-95 levels. Importantly, an RPS23RG1-derived peptide comprising a unique PSD-93/PSD-95 interaction motif rescued synaptic and cognitive defects in *Rps23rg1* KO and AD mouse models.

**CONCLUSIONS:** Our results reveal a role for RPS23RG1 in maintaining synaptic integrity and function and provide a new mechanism for synaptic dysfunction in AD pathogenesis. This demonstrates that RPS23RG1-mediated pathways show good therapeutic potential in AD intervention.

### Keywords

Alzheimer's disease; PSD-93; PSD-95; RPS23RG1; Synaptic plasticity; Ubiquitination

## INTRODUCTION

Synaptic dysfunction is a causal factor in memory impairment in Alzheimer's disease (AD) (1–3). The scaffolding protein PSD-95 localizes to post-synaptic densities (PSDs) and plays an important role in organizing neuro-signaling factors (4, 5). Deletion or dysregulation of PSD-95 and the related scaffolding protein PSD-93 impairs synaptic function, with consequent effects on learning and memory (6–9). PSD-95 and PSD-93 levels have been reported to be decreased in human AD and in AD mouse models (10–12), suggesting that synaptic dysfunction is a consequence of dysregulated homeostasis of PSD scaffolding components.

The turnover of PSD-95 is through the ubiquitin-proteasome system (UPS) (13, 14). UPS is critical for regulating the protein milieu within neurons, and specifically modulates the compositional landscape within PSDs (15, 16). The E3 ubiquitin ligase MDM2 (murine double minute 2) can mediate PSD-95 turnover, where proteosomal PSD-95 regulation is required to modulate surface glutamate receptor levels in synaptic plasticity (14). Given that ubiquitin-associated pathology is commonly observed in AD (17), it is plausible that UPS-dependent dysregulation of PSD components plays a role in AD pathogenesis. However, molecular mechanisms underlying PSD dysregulation remain largely unclear.

AD features the pathological formation of  $\beta$ -amyloid ( $A\beta$ )-enriched plaques and neurofibrillary tangles comprising hyperphosphorylated tau (18). The *Rps23rg1* gene (ribosomal protein S23 retroposed gene) was recently identified through a genetic screen for anti- $A\beta$  components. RPS23RG1 is a transmembrane protein which can concurrently inhibit  $A\beta$  generation and tau hyperphosphorylation through interactions with adenylyl cyclases, thereby enhancing cAMP/PKA to inhibit GSK3 activity (19). The RPS23RG family is conserved in both mouse and human, with two functionally expressed genes in mouse (*Rps23rg1* and *Rps23rg2*) and one functionally expressed gene (*RPS23RG1*) identified in

human so far (19–21). Until now, the physiological function of RPS23RG family members remains elusive.

## METHODS AND MATERIALS

Plasmids, antibodies and primers are discussed in Supplemental Methods and Materials.

### Animals

C57BL/6 mice were from Xiamen University Laboratory Animal Center (Xiamen, China). APP/PS1 AD model mice (22, 23) were from Model Animal Research Center of Nanjing University (Nanjing, China). *Rps23rg1* knockout (KO) mice were generated as discussed in Supplemental Methods and Materials. Animal experiments were approved by and conducted in accordance with the guidelines of the Animal Ethics Committee of Xiamen University.

### PSD Fraction Preparation

PSD fractions from mouse hippocampus were dissected as previously described (24, 25).

### Cell Culture and Transfection

HEK293T cells and mouse primary neurons were cultured as previously reported (26) and transfected using Turbofect (Thermo Fisher Scientific, Waltham, MA, USA) or Lipofectamine 2000 (Thermo Fisher Scientific) reagents.

### Protein Degradation Assays

Wild type (WT) and *Rps23rg1* KO mouse primary neurons were treated with cycloheximide (Sigma-Aldrich, St. Louis, MO, USA) for indicated time periods. Alternatively, neurons were treated with cycloheximide in the presence of the proteosomal inhibitor MG132 (APExBIO, Houston, TX, USA) for 16 h.

### Biotinylation

Cell surface protein biotinylation was performed as previously described (27).

### Western Blot and Co-immunoprecipitation

Samples were lysed in TNE buffer (26). Protein lysates were immunoblotted with indicated antibodies. For co-immunoprecipitation, 1 mg protein lysates were incubated with 1–2 µg indicated antibodies or IgG and 25 µl Protein G-Agarose beads (Roche Diagnostics Ltd, Shanghai, China) at 4°C overnight. Immunocomplexes were analyzed by immunoblotting. Protein band intensity was quantified using the ImageJ software.

### Immunocytochemistry

Immunocytochemistry was performed as previously described (20). Samples were visualized under a confocal fluorescence microscope (Nikon, Japan). PSD-93 and PSD-95 cluster numbers in neurons were counted.

## Golgi Staining and Analysis

Mouse brains were dissected and treated with the FD Rapid Golgostain™ Kit (FD NeuroTechnologies, Shanghai, China) following the manufacturer's instructions. Slices were visualized under a confocal microscope. Images were captured from Golgi-impregnated hippocampal CA1 pyramidal neurons. Z-stack-compressed TIFF files were imported into ImageJ. Images were calibrated according to the acquisition parameters and spine numbers were counted.

## Electron Microscope Analysis

Synapse structures were analyzed using transmission electron microscope as previously described (28).

## Behavioral Experiments

Experimental details for mouse behavioral analysis are discussed in Supplemental Methods and Materials.

## Electrophysiological Recording

Electrophysiological recordings were performed as previously described (29, 30).

## Brain Ventricle Virus Injections

Adenoviruses expressing PSD-95 and control GFP were from Vigene Biosciences (Jinan, China). Lentiviruses expressing PSD-93 and control GFP were from Genechem (Shanghai, China). *Rps23rg1* KO mice at P0 were bilaterally co-injected with control adenovirus and control lentivirus, control adenovirus and lentivirus expressing PSD-93, control lentivirus and adenovirus expressing PSD-95, or lentivirus expressing PSD-93 and adenovirus expressing PSD-95. Mice were analyzed for behaviors at 2-months-old and sacrificed for electrophysiological and biochemical analyses.

## Human RPS23RG1 Intracellular Domain Peptide Design and Administration

The human RPS23RG1 intracellular domain (ICD, sequence corresponding to the last 19 amino acids of RPS23RG1 carboxyl-terminus) was used as the peptide core. A scrambled (Scb) control comprising the same 19 amino acids with a scrambled sequence order was also used. Peptide cores were conjugated with a biotin or a fluorescein isothiocyanate (FITC) moiety bridged with a GGG linker at their amino-termini, and/or conjugated to an 11-amino acid-long peptide derived from the transactivator of transcription (TAT) protein at their carboxyl-termini. Conjugated peptide sequences were as follows:

```
[FITC]ICD-TAT: [FITC]GGGETPSSMRSTTLAHPAVLRAYARAARRAARR;
[FITC]Scb-TAT: [FITC]GGGSTRMSSPTEARLVAPHALTYARAARRAARR;
[biotin]ICD-TAT: [biotin]ETPSSMRSTTLAHPAVLRAYARAARRAARR;
[biotin]Scb-TAT: [biotin]STRMSSPTEARLVAPHALTYARAARRAARR;
[biotin]ICD: [biotin]ETPSSMRSTTLAHPAVLRA.
```

Peptides were synthesized by GL Biochem (Shanghai, China). Following a previously described procedure (31), peptides were dissolved in a saline buffer and intraperitoneally (i.p.) injected into mice at a dose of 40 mg/kg/d for three consecutive days. Mice were then subjected to behavioral, electrophysiological and biochemical analyses.

## Statistics

All data represent mean  $\pm$  s.e.m. Statistical analyses were performed using Graphpad Prism or Origin softwares. Detailed statistical analysis methods for each comparison are indicated in the text.

## RESULTS

### ***Rps23rg1* KO Mice Exhibit Severe Cognitive and Synaptic Plasticity Deficits**

Mouse *Rps23rg1* was expressed in all tissues examined, including cortex, hippocampus and cerebellum (Supplemental Figures S1A and S1B). In the brain, RPS23RG1 was expressed in neurons as well as in microglia and astrocytes (Supplemental Figure S1C). Furthermore, RPS23RG1 was distributed to synaptosomes/PSD-enriched fractions in a pattern similar to PSD-95 (Supplemental Figure S1D).

We generated an *Rps23rg1* KO mouse line that comprises a five nucleotide “ACTTC” deletion within the *Rps23rg1* protein coding sequence, resulting in a frame shift and early truncation of RPS23RG1 (Supplemental Figures S2A-D). *Rps23rg1* mRNA (Supplemental Figure S2E) and protein levels (Supplemental Figure S2F) were undetectable in homozygous *Rps23rg1* KO mouse brain. Homozygous *Rps23rg1* KO mice were born at an expected Mendelian frequency and with a ~1:1 sex ratio (Supplemental Figure S2G), and featured normal overall physiology with comparable body weight to WT littermate controls (Supplemental Figure S2H). No appreciable differences in cortical and hippocampal structure and neuron abundance were apparent comparing *Rps23rg1* KO and WT mouse brain sections (Supplemental Figures S2I and S2J). These results suggest that *Rps23rg1* is not essential for normal development in mice.

RPS23RG1 is abundant in the hippocampus and synaptosomes, implicating a potential role for RPS23RG1 in synaptic plasticity and cognition. We observed that *Rps23rg1* KO mice featured slightly lower locomotor activity compared to WT controls in open field tests, but there were no differences in their time spent in central areas (Supplemental Figure S3A), implying that loss of *Rps23rg1* had little effect on mouse anxiety. However, in T-maze tests, *Rps23rg1* KO mice showed significantly reduced spontaneous alternations compared to WT mice (Figure 1A). In novel object recognition memory tests, although both *Rps23rg1* KO and WT mice exhibited similar exploration time with two identical objects during the training phase, only WT mice explored novel objects comparatively more than familiar objects during the testing phase, whereas *Rps23rg1* KO mice explored novel and familiar objects without discrimination (Supplemental Figure S3B). These differences led to a significantly lower discrimination index in *Rps23rg1* KO mice than controls (Figure 1B).

In fear conditioning tests, freezing levels in *Rps23rg1* KO and WT mice were similar during habituation and conditioning trials (Supplemental Figure S3C). However, *Rps23rg1* KO

mice showed significantly lower freezing percentages compared to controls when contextual and cued fear memories were tested 24 h later (Figure 1C). Moreover, although both *Rps23rg1* KO and WT mice showed progressive decline in escape latency during a seven-day training phase in Morris water maze tests, *Rps23rg1* KO mice showed reduced escape latency declination compared to controls (Figure 1D, left panel). During probe trial tests, *Rps23rg1* KO mice spent significantly less time in the target quadrant (Figure 1D, middle panel), and demonstrated fewer platform location crossings than controls (Figure 1D, right panel). These results demonstrate that *Rps23rg1* mediates a broad range of cognition-related behaviors and its loss severely impairs learning and memory.

When whole-cell mEPSC (miniature excitatory postsynaptic current) recordings were performed to determine synaptic function mediated by AMPA ( $\alpha$ -amino-3-hydroxy-5-methyl-4-isoxazolepropionic acid) and NMDA (*N*-methyl D-aspartate) receptors (Supplemental Figures S4A and S4B), both AMPA and NMDA receptor-mediated mEPSC amplitudes were dramatically reduced in CA1 pyramidal neurons derived from *Rps23rg1* KO mice compared to controls (Supplemental Figures S4C and S4D), indicating defects in postsynaptic glutamatergic transmission. Interestingly, AMPA and NMDA-associated mEPSC frequencies were also reduced in *Rps23rg1* KO neurons (Supplemental Figures S4C and S4D), denoting defects in presynaptic glutamate release or a reduction in synaptic abundance. Given that paired-pulse facilitation did not vary significantly between *Rps23rg1* KO and WT mice (Supplemental Figure S4E), mEPSC frequency attenuation is likely induced by a reduction in functional synapses. In addition, the amplitude of evoked EPSCs mediated by both AMPA and NMDA receptors were lower in *Rps23rg1* KO mouse CA1 neurons than in controls (Supplemental Figures S4F and S4G). A marked reduction in fEPSP slopes from *Rps23rg1* KO mouse hippocampus was detected in the CA1 stratum radiatum with progressively increased stimulation of the Schaffer collateral (SC)/commissural pathway (Figure 1E). LTP response was also attenuated within the SC-CA1 region in *Rps23rg1* KO mice (Figure 1F). Together, these results indicate that loss of *Rps23rg1* impairs postsynaptic glutamatergic neurotransmission and synaptic function.

### ***Rps23rg1* Deletion Renders Defects in Synaptic Structure and Composition**

A significant reduction in the number of mature spines was observed in *Rps23rg1* KO animals within the CA1 region (Figure 2A), and in cultured primary neurons (Figure 2B). Immunocytochemistry results revealed a marked reduction in co-clusters of the pre-synaptic marker synaptophysin and the post-synaptic marker PSD-95, implying a reduction in synapses in *Rps23rg1* KO neurons (Figure 2C). Electron microscopy analyses also showed reductions in PSD length and width in *Rps23rg1* KO mice (Figure 2D), indicative of structural synaptic defects in the absence of *Rps23rg1*.

Given that PSD-93 and PSD-95 are key scaffolding components at PSDs, structural defects in *Rps23rg1* KO neurons may be derived from perturbations in PSD-93/PSD-95. Indeed, we observed reduced PSD-93 and PSD-95 protein levels in *Rps23rg1* KO mouse brain (Figure 3A), as well as synaptosome and PSD-enriched fractions from *Rps23rg1* KO brain hippocampus (Figure 3B). PSD-93- and PSD-95-staining intensity was also reduced in cultured *Rps23rg1* KO primary neurons (Figure 3C). Loss of *Rps23rg1* had no effect on



PSD-93 and PSD-95 mRNA expression (Supplemental Figure S5), suggesting that *Rps23rg1* affects posttranslational PSD-93/95 stability or turnover. When protein synthesis was inhibited by cycloheximide, we indeed observed accelerated PSD-93 and PSD-95 turnover in *Rps23rg1* KO neurons (Figure 3D). These results implicate an essential role for *Rps23rg1* in maintaining PSD-93/PSD-95 protein levels.

Both PSD-93 and PSD-95 interact with glutamate receptors, thereby regulating their trafficking to consequently modulate synaptic plasticity (9, 32–37). Consistent with PSD-93 and PSD-95 reductions, cell surface distributions of the AMPAR subunit GluA1 and the NMDAR subunit GluN1 were markedly decreased in *Rps23rg1* KO mouse primary neurons (Figure 3E). These results demonstrate that *Rps23rg1* deletion is associated with reductions in PSD-93/PSD-95 and surface glutamate receptor levels which may compromise synaptic plasticity.

### **RPS23RG1 Interacts with and Stabilizes PSD-93 and PSD-95 by Attenuating MDM2-Mediated PSD-93/PSD-95 Turnover**

MDM2 mediates PSD-95 poly-ubiquitination and degradation (14). As expected, exposure to the proteasomal inhibitor MG132 stabilized PSD-95 as well as PSD-93 in neurons treated with cycloheximide (Figure 4A). In addition, PSD-93 and PSD-95 immunoprecipitates associated with higher levels of high-molecular weight PSD-93/PSD-95 poly-ubiquitin conjugates in *Rps23rg1* KO mouse brain compared to controls (Figure 4B).

Notably, we found that endogenous PSD-93 and PSD-95 was co-precipitated with an RPS23RG1 antibody in WT but not *Rps23rg1* KO mouse brain lysates (Figure 4C). No interaction was observed between RPS23RG1 and other PSD-93/PSD-95 related DLG-family proteins such as SAP97 and SAP102 (Figure 4C). RPS23RG1 is a type Ib transmembrane protein comprising ~60% homology in human and mouse (Supplemental Figure S6A). Recombinant human RPS23RG1 also co-precipitated with PSD-93 and PSD-95 but not with SAP97 or SAP102 from WT mouse brain lysates (Supplemental Figure S6B). Moreover, RPS23RG1 co-localized with PSD-93 and PSD-95 puncta in cultured primary neurons (Figure 4D). Using deletion constructs within the intracellular domain (Figure 4E and Supplemental Figure S6C), we identified a conserved “TTLAH” motif present in both human (aa163–167) and mouse (aa130–134) RPS23RG1 as an essential region for RPS23RG1-PSD-93 and RPS23RG1-PSD-95 interactions; deletion of this motif in human RPS23RG1 abrogated its interaction with PSD-93 and PSD-95 (Figure 4F). Similarly, deletion of human and mouse carboxyl-terminal regions spanning this motif also abrogated their interactions with PSD-93/PSD-95 (Figure 4F and Supplemental Figure S6D).

We originally postulated that RPS23RG1 could modulate PSD-93/PSD-95 ubiquitination by binding MDM2; however, we were unable to detect interactions between MDM2 and RPS23RG1 (Supplemental Figure S7A). Rather, we found that RPS23RG1 overexpression attenuated MDM2 interactions with PSD-93 and PSD-95 in a dose-dependent manner (Supplemental Figures S7B and S7D), while dose-dependent MDM2 overexpression also attenuated RPS23RG1-PSD-93 and RPS23RG1-PSD-95 interactions (Supplemental Figures S7C and S7E). Moreover, overexpression of full-length human RPS23RG1 but not

RPS23RG1 lacking the intracellular domain markedly reversed PSD-93 and PSD-95 poly-ubiquitination induced by MDM2 overexpression (Supplemental Figures S7F and S7G). These results suggest that MDM2 and RPS23RG1 compete for PSD-93/PSD-95 interactions. To confirm these results *in vivo*, we characterized PSD-93/PSD-95 interactions with MDM2 from WT and *Rps23rg1* KO mouse brain, and found that *Rps23rg1* deletion indeed enhanced MDM2 co-immunoprecipitation with PSD-93 and PSD-95 in total brain lysates and synaptosomes (Figure 4G).

### Restoration of PSD-95 and PSD-93 Levels Rescues Cognitive and Synaptic Deficits in *Rps23rg1* KO Mice

We injected viruses expressing PSD-93 (lentivirus) and/or PSD-95 (adenovirus) bilaterally into lateral ventricles of P0 mice to normalize PSD-93 and/or PSD-95 expression (Figure 5A). Mouse behaviors were assayed at 2 month of age. Although expression of PSD-93 or PSD-95 individually in *Rps23rg1* KO mice showed no effect on improving cognitive behavior, PSD-93/PSD-95 co-expression rescued the reduced discrimination index in both objection location memory (Figure 5B) and novel object recognition memory tests (Figure 5C). *Rps23rg1* deletion abrogated novel arm explorations within a modified T-maze; while combinatorial PSD-93 and PSD-95 expression in *Rps23rg1* KO mice rescued reductions in novel arm exploration, and nearly restored reduced entries into the novel arm (Figure 5D). Moreover, overexpression of PSD-93 and/or PSD-95 ameliorated impaired LTP response in *Rps23rg1* KO hippocampus (Figure 5E). These results indicate that restoring PSD-93 and PSD-95 levels can rescue synaptic and cognitive impairments in *Rps23rg1* KO mice.

### A PSD-Stabilizing RPS23RG1 Peptide Rescues Cognitive and Synaptic Deficits in *Rps23rg1* KO Mice

Since RPS23RG1 binds PSD-93 and PSD-95 through a unique sequence within the intracellular domain (ICD), it may be possible to displace PSD-destabilizing MDM2-PSD-93 and MDM2-PSD-95 interactions using a competing RPS23RG1 ICD peptide. To test this, we conjugated the carboxyl-terminus of the 19aa RPS23RG1 ICD sequence comprising the “TTLAH” PSD-93/PSD-95 binding motif, or a control scrambled (Scb) peptide to a TAT transduction sequence to facilitate intracellular uptake (31). Peptide amino-terminus was conjugated with biotin or FITC with an adjoining glycine linker. To evaluate peptide permeability through the BBB with peripheral injection, <sup>125</sup>I-labeled [biotin]ICD-TAT peptides were injected into WT mice through i.p. administration. Approximately 0.220 ± 0.046% of the injected peptide was detected in the brain 30 min following i.p. administration. Moreover, 24 hours following i.p. injection of different peptides, the [biotin]ICD-TAT peptide was found to co-precipitate both PSD-93 and PSD-95, while the [biotin]ICD peptide (no TAT) precipitated much less PSD-93/PSD-95 compared to [biotin]ICD-TAT (Figure 6A). No PSD-93/PSD-95 co-precipitation was observed with [biotin]Scb-TAT injection from brain lysates (Figure 6A). These results demonstrate that the ICD-TAT peptide can penetrate the BBB and successfully target PSD-93 and PSD-95.

We i.p. injected FITC-conjugated ICD-TAT and Scb-TAT peptides into *Rps23rg1* KO mice at a dose of 40 mg/kg/d for three consecutive days, whereby mice were subjected to behavioral, electrophysiological and biochemical analyses (Supplemental Figure S8A). We



found no variable effects on animal body weight with peptide injection (Supplemental Figure S8B). FITC signals were detected in the cortex and hippocampus of treated mice, indicating BBB penetration of these peptides (Supplemental Figures S8C and S8D). Importantly, ICD-TAT treatment in *Rps23rg1* KO mice rescued spontaneous alternation deficits in T-maze tests (Figure 6B) and reversed impaired discrimination indexes in novel object recognition memory tests (Figure 6C). ICD-TAT treatment also enhanced LTP in *Rps23rg1* KO mouse SC-CA1 hippocampus (Figure 6D). Moreover, ICD-TAT treatment increased PSD-93 and PSD-95 protein levels in *Rps23rg1* KO mouse brain, attenuated MDM2-PSD-93 and MDM2-PSD-95 interactions (Figure 6E), and reduced PSD-93 and PSD-95 poly-ubiquitination (Figures 6F and 6G). These results indicate that the human RPS23RG1 ICD-TAT peptide can reverse synaptic and cognitive deficits in *Rps23rg1* KO mice.

### **RPS23RG1 Expression is Attenuated in Human AD and Correlates with PSD-93 and PSD-95 Levels**

We found that *RPS23RG1* mRNA expression was dramatically decreased in postmortem AD brain compared to controls (Figure 7A). Interestingly, RPS23RG1 protein levels positively correlated with PSD-93 and PSD-95 protein levels in AD samples (Figure 7B). Similarly, we observed a reduction in *Rps23rg1* mRNA levels in aged APP/PS1 AD mouse brain (Figure 7C), and found that RPS23RG1, PSD-93 and PSD-95 levels declined at 7 months of age (Figure 7D) in APP/PS1 mice when disease-associated phenotypes initially manifest (23). These results suggest a working model where RPS23RG1 reduction can promote PSD-93/PSD-95 destabilization and turnover to trigger cognitive impairment with AD onset.

### **The PSD-Stabilizing RPS23RG1 Peptide Rescues Cognitive and Synaptic Deficits in APP/PS1 Mice**

Similar to our results in *Rps23rg1* KO mice, peripheral injection of 7-month-old APP/PS1 mice with ICD-TAT peptides restored PSD-93 and PSD-95 levels (Figure 8A). ICD-TAT injection in APP/PS1 mice also rescued spontaneous alternation deficits in T-maze tests (Figure 8B), reversed memory impairment in object location memory tests (Figure 8C) and had memory improvement tendency in novel object recognition memory tests (Figure 8D). Impaired LTP response in APP/PS1 animals was improved upon ICD-TAT injection (Figure 8E). ICD-TAT peptide treatment in APP/PS1 mice did not affect tau phosphorylation (Supplemental Figures S9A and S9B) or A $\beta$  levels (Supplemental Figure S9C), and had little effect on PKA-mediated phosphorylation of GluA1 on S845, which was previously shown to modulate subcellular GluA1 trafficking and activity (38–40) (Supplemental Figures S9A and S9B). Given that RPS23RG1 regulates A $\beta$  generation and tau phosphorylation mainly through transmembrane domain interactions with adenylyl cyclases to enhance downstream signaling pathways (21), it may be expected that RPS23RG1 ICD will have little or no effect on adenylyl cyclase-associated A $\beta$  and tau pathways. Moreover, ICD-TAT peptide treatment did not affect GFAP or Iba-1 levels (Supplemental Figures S9A and S9B), suggesting that ICD-TAT peptide treatment does not trigger a neuro-inflammatory response. Hence, restoration of PSD-destabilizing defects associated with RPS23RG1 can reverse synaptic and cognitive impairments in AD.

## DISCUSSION

Here, we present a model for RPS23RG1-mediated synaptic stabilization through interactions between the RPS23RG1 ICD and PSD-93/PSD-95, thereby displacing MDM2-PSD-93 and MDM2-PSD-95 binding and consequent poly-ubiquitination/degradation (Supplemental Figure S10). Proper homeostatic maintenance of PSD components is fundamental to the function and distribution of various ionotropic receptors at the post-synaptic compartment. For example, PSD-95 can interact directly with NMDARs and indirectly with AMPARs through Stargazin/TARPs, and thus modulate these receptors' trafficking and synaptic plasticity (32–35). Therefore, alterations in mechanisms that regulate PSD scaffolding component homeostasis may have a significant impact on synaptic function and consequent cognitive behavior.

Indeed, previous studies have reported decreased PSD-95 levels in human AD brain and in AD mouse models, which correlate with increasing pathological severity and dementia (41–45). Although some studies have reported contradictory results indicating that PSD-95 levels may be increased in human AD (46, 47), compensatory changes may be involved at certain stages during AD onset (10). Interestingly, one particular report suggests that PSD components are upregulated in early Braak stages (I-III), and downregulated in late stages (IV-VI) (11). This indicates that restoration of PSD function may be dependent on pathological severity during AD progression. In support of this, upregulation of PSD-95 expression through epigenetic targeting and modification of the PSD-95 locus restored cognition in APP/PS1 mice (48). Restoration of PSD-93 levels in APP/PS1 AD mouse hippocampus through lentiviral-mediated expression also attenuated impairment in spatial learning and memory (49). As our results similarly indicate that stabilization of PSD components such as PSD-93/PSD-95 through an RPS23RG1-derived ICD peptide can restore synaptic and cognitive deficits in APP/PS1 mice, reconstituting depleted PSD components may be a good complementary strategy to reverse neuronal impairment in late AD.

In addition to neurons, RPS23RG1 is expressed in microglia and astrocytes. One recent study found that PSD-95 could be detected in microglia derived from P1 mice by immunofluorescent staining, where PSD-95 levels disappeared by P3, suggesting that PSD-95 is involved in early brain development (50). Although we could not detect PSD-95 in P1 murine microglia by immunoblotting, we do not discount the possibility that RPS23RG1 may also modulate PSD-95-dependent microglia function in brain development.

Since the “TTLAH” motif is crucial for RPS23RG1 interactions with PSD-93/PSD-95, we used BLAST to search for human and mouse protein sequences within the GenBank database and identified 151 candidate proteins comprising this motif. However, we detected no interaction between one of these candidate proteins, KCNH5 (potassium voltage-gated channel subfamily H member 5, also known as Kv10.2 and EAG2) and PSD-95 (Supplemental Figure S11). This is consistent with previous reports describing little or no colocalization between KCNH5 and PSD-95 in hippocampal neurons (51). Together, this suggests that although the “TTLAH” motif is necessary for RPS23RG1-PSD-95 interaction, other RPS23RG1 domain(s) may also be required for binding, possibly by forming a

specialized spatially-defined three dimensional structure with the “TTLAH” motif to accommodate PSD-95 interaction.

Since both A $\beta$  proteotoxicity and A $\beta$ -mediated synaptic dysfunction are key events in cognitive decline and AD progression (52, 53), impairment of mechanisms that concurrently influence amyloidogenic A $\beta$  production/accumulation and synaptic dysregulation may be critical triggers in AD onset. Given that our previous results implicate a role for RPS23RG1 in inhibiting A $\beta$  generation through adenylyl cyclase/PKA activation and consequent GSK3 inhibition (19, 20), together with our results here demonstrating a physiological role for RPS23RG1 in binding and stabilizing PSD components, RPS23RG1 reduction in AD could simultaneously enhance A $\beta$  proteotoxicity and drive synaptic degeneration. In addition, we noticed that A $\beta$  treatment markedly reduced RPS23RG1 levels (Supplemental Figures S12A and S12B), whereas tau overexpression showed little or no effect (Supplemental Figure S12C). These findings suggest that RPS23RG1 downregulation contributes significantly to AD pathogenesis: RPS23RG1 impairment potentially triggered by A $\beta$  toxicity, may enhance A $\beta$  production as well as tau hyperphosphorylation at early stages of AD, resulting in cyclical acceleration of neurodegenerative progression. During this process, reductions in RPS23RG1 would also impair synaptic structure and function through PSD-93/PSD-95 destabilization.

Given that restoration or enhancement of RPS23RG1 pathways can selectively limit amyloidogenic A $\beta$  accumulation, synaptic impairment, or target both pathogenic features, RPS23RG1 may be a pharmacological target of particular interest in AD. Future work will determine whether modulation of RPS23RG1 can confer long-term preventative and restorative effects in AD.

Our results here also provide a new mechanism underlying PSD destabilization and turnover through the ubiquitin/proteasome pathway. Defects in synaptic stability, homeostasis, and PSD composition have also been described in other neurodegenerative disorders. For example, decreased PSD-95 levels have been observed in the striatal region of Huntington’s disease (HD) patients (54). Although HD mouse brain features increased spine formation, HD mice also show defects in dendritic spine stability and maturation (55). Decreased spine density has also been noted in Parkinson’s disease (56), and synaptic loss has been observed in mouse models of amyotrophic lateral sclerosis (57). Although PSD-95 homeostasis involves MDM2-mediated poly-ubiquitination and turnover (14), how this mechanism can affect synaptic formation and function in various neurodegenerative disorders was unclear. Since RPS23RG1 can restore dysregulated synaptic function in AD by attenuating MDM2-dependent PSD-93/PSD-95 turnover, it will be interesting to determine whether impaired *Rps23rg1* function is apparent in other neurodegenerative disorders, and importantly, assess whether enhancing RPS23RG1-associated PSD-93/PSD-95 stability can reverse synaptic deficits in these disorders.

## Supplementary Material

Refer to Web version on PubMed Central for supplementary material.

## ACKNOWLEDGEMENTS AND DISCLOSURES

This work was supported in part by grants from The National Key Research and Development Program of China (2016YFC1305903), The National Natural Science Foundation of China (91332112, U1705285, 81225008, and 81771377 to Y-w.Z., U1405222 to H.X., and 81774377 and 81373999 to L.W.), National Institutes of Health (R01AG021173, R01AG038710, R01AG044420, and R01NS046673 to H.X.), Fundamental Research Funds for the Central Universities (20720180049 to Y-w.Z.), Xiamen Science and Technology Program for Public Wellbeing (3502Z20174067 to F-r.L.), and Natural Science Foundation of Guangdong Province of China (2018A030313158 to Y.L.).

We would like to thank Dr. Xianzhong Zhang for helpful discussion, and Drs. Eliezer Masliah and Robert A. Rissman for providing AD patient and control samples.

D.Z. contributed to the design, execution, analysis and interpretation of the studies and drafting of the manuscript; J.M. helped on plasmid construction and animal maintenance and behavioral tests; Y.Z. and T.Z. helped on RPS23RG1 expression in AD patients; Y.H. helped on peptide treatments and animal behavioral tests; Y.L., N.Z., Y.G., and Z.C. performed electrophysiological studies under the guidance of H.S., L.W. and Y.L.; M.Z. and C.J. provided technical support; X.W. performed studies on peptide labeling and BBB passage; X.Z., H.L., X.W., J.Z., F-r.L., and G.B. helped interpreting experiments; T.Y.H. aided in interpreting the experiments and writing the manuscript; H.X. designed, interpreted and wrote the manuscript; Y-w.Z. designed, interpreted and supervised the entire study and wrote the manuscript.

## REFERENCES

- Koffie RM, Hyman BT, Spiess-Jones TL (2011): Alzheimer's disease: synapses gone cold. *Mol Neurodegener* 6:63. [PubMed: 21871088]
- Shankar GM, Walsh DM (2009): Alzheimer's disease: synaptic dysfunction and Abeta. *Mol Neurodegener* 4:48. [PubMed: 19930651]
- Audrain M, Fol R, Dutar P, Potier B, Billard JM, Flament J, et al. (2016): Alzheimer's disease-like APP processing in wild-type mice identifies synaptic defects as initial steps of disease progression. *Mol Neurodegener* 11:5. [PubMed: 26759118]
- Zhu J, Shang Y, Zhang M (2016): Mechanistic basis of MAGUK-organized complexes in synaptic development and signalling. *Nat Rev Neurosci* 17:209–223. [PubMed: 26988743]
- Elias GM, Funke L, Stein V, Grant SG, Brecht DS, Nicoll RA (2006): Synapse-specific and developmentally regulated targeting of AMPA receptors by a family of MAGUK scaffolding proteins. *Neuron* 52:307–320. [PubMed: 17046693]
- Nithianantharajah J, Komiyama NH, McKechnie A, Johnstone M, Blackwood DH, St Clair D, et al. (2013): Synaptic scaffold evolution generated components of vertebrate cognitive complexity. *Nat Neurosci* 16:16–24. [PubMed: 23201973]
- Carlisle HJ, Fink AE, Grant SG, O'Dell TJ (2008): Opposing effects of PSD-93 and PSD-95 on long-term potentiation and spike timing-dependent plasticity. *J Physiol* 586:5885–5900. [PubMed: 18936077]
- Migaud M, Charlesworth P, Dempster M, Webster LC, Watabe AM, Makhinson M, et al. (1998): Enhanced long-term potentiation and impaired learning in mice with mutant postsynaptic density-95 protein. *Nature* 396:433–439. [PubMed: 9853749]
- Tao YX, Rumbaugh G, Wang GD, Petralia RS, Zhao C, Kauer FW, et al. (2003): Impaired NMDA receptor-mediated postsynaptic function and blunted NMDA receptor-dependent persistent pain in mice lacking postsynaptic density-93 protein. *J Neurosci* 23:6703–6712. [PubMed: 12890763]
- Savioz A, Leuba G, Vallet PG (2014): A framework to understand the variations of PSD-95 expression in brain aging and in Alzheimer's disease. *Ageing Res Rev* 18:86–94. [PubMed: 25264360]
- Hondius DC, van Nierop P, Li KW, Hoozemans JJ, van der Schors RC, van Haastert ES, et al. (2016): Profiling the human hippocampal proteome at all pathologic stages of Alzheimer's disease. *Alzheimers Dement* 12:654–668. [PubMed: 26772638]
- Shao CY, Mirra SS, Sait HB, Sacktor TC, Sigurdsson EM (2011): Postsynaptic degeneration as revealed by PSD-95 reduction occurs after advanced Abeta and tau pathology in transgenic mouse models of Alzheimer's disease. *Acta Neuropathol* 122:285–292. [PubMed: 21630115]

13. Vallejo D, Codocedo JF, Inestrosa NC (2017): Posttranslational Modifications Regulate the Postsynaptic Localization of PSD-95. *Mol Neurobiol* 54:1759–1776. [PubMed: 26884267]
14. Colledge M, Snyder EM, Crozier RA, Soderling JA, Jin Y, Langeberg LK, et al. (2003): Ubiquitination regulates PSD-95 degradation and AMPA receptor surface expression. *Neuron* 40:595–607. [PubMed: 14642282]
15. Caldeira MV, Salazar IL, Curcio M, Canzoniero LM, Duarte CB (2014): Role of the ubiquitin-proteasome system in brain ischemia: friend or foe? *Prog Neurobiol* 112:50–69. [PubMed: 24157661]
16. Ehlers MD (2003): Activity level controls postsynaptic composition and signaling via the ubiquitin-proteasome system. *Nat Neurosci* 6:231–242. [PubMed: 12577062]
17. Ciechanover A, Kwon YT (2015): Degradation of misfolded proteins in neurodegenerative diseases: therapeutic targets and strategies. *Exp Mol Med* 47:e147. [PubMed: 25766616]
18. Giacobini E, Gold G (2013): Alzheimer disease therapy--moving from amyloid-beta to tau. *Nat Rev Neurol* 9:677–686. [PubMed: 24217510]
19. Zhang YW, Liu S, Zhang X, Li WB, Chen Y, Huang X, et al. (2009): A functional mouse retroposed gene *Rps23r1* reduces Alzheimer's beta-amyloid levels and tau phosphorylation. *Neuron* 64:328–340. [PubMed: 19914182]
20. Yan L, Chen Y, Li W, Huang X, Badie H, Jian F, et al. (2016): *RPS23RG1* reduces Abeta oligomer-induced synaptic and cognitive deficits. *Sci Rep* 6:18668. [PubMed: 26733416]
21. Huang X, Chen Y, Li WB, Cohen SN, Liao FF, Li L, et al. (2010): The *Rps23rg* gene family originated through retroposition of the ribosomal protein *s23* mRNA and encodes proteins that decrease Alzheimer's beta-amyloid level and tau phosphorylation. *Hum Mol Genet* 19:3835–3843. [PubMed: 20650958]
22. Jankowsky JL, Slunt HH, Ratovitski T, Jenkins NA, Copeland NG, Borchelt DR (2001): Co-expression of multiple transgenes in mouse CNS: a comparison of strategies. *Biomol Eng* 17:157–165. [PubMed: 11337275]
23. Reiserer RS, Harrison FE, Syverud DC, McDonald MP (2007): Impaired spatial learning in the APPSwe + PSEN1DeltaE9 bigenic mouse model of Alzheimer's disease. *Genes Brain Behav* 6:54–65. [PubMed: 17233641]
24. Seo J, Giusti-Rodriguez P, Zhou Y, Rudenko A, Cho S, Ota KT, et al. (2014): Activity-dependent p25 generation regulates synaptic plasticity and Abeta-induced cognitive impairment. *Cell* 157:486–498. [PubMed: 24725413]
25. Chao HW, Tsai LY, Lu YL, Lin PY, Huang WH, Chou HJ, et al. (2013): Deletion of *CPEB3* enhances hippocampus-dependent memory via increasing expressions of PSD95 and NMDA receptors. *J Neurosci* 33:17008–17022. [PubMed: 24155305]
26. Zheng Q, Zheng X, Zhang L, Luo H, Qian L, Fu X, et al. (2017): The Neuron-Specific Protein *TMEM59L* Mediates Oxidative Stress-Induced Cell Death. *Mol Neurobiol* 54:4189–4200. [PubMed: 27324899]
27. Wang X, Zhao Y, Zhang X, Badie H, Zhou Y, Mu Y, et al. (2013): Loss of sorting nexin 27 contributes to excitatory synaptic dysfunction by modulating glutamate receptor recycling in Down's syndrome. *Nat Med* 19:473–480. [PubMed: 23524343]
28. Ung DC, Iacono G, Meziane H, Blanchard E, Papon MA, Selten M, et al. (2017): *Ptchd1* deficiency induces excitatory synaptic and cognitive dysfunctions in mouse. *Mol Psychiatry*.
29. Wen L, Lu YS, Zhu XH, Li XM, Woo RS, Chen YJ, et al. (2010): Neuregulin 1 regulates pyramidal neuron activity via ErbB4 in parvalbumin-positive interneurons. *Proceedings of the National Academy of Sciences of the United States of America* 107:1211–1216. [PubMed: 20080551]
30. Wen L, Tang FL, Hong Y, Luo SW, Wang CL, He W, et al. (2011): *VPS35* haploinsufficiency increases Alzheimer's disease neuropathology. *The Journal of cell biology* 195:765–779. [PubMed: 22105352]
31. Shukla V, Zheng YL, Mishra SK, Amin ND, Steiner J, Grant P, et al. (2013): A truncated peptide from p35, a *Cdk5* activator, prevents Alzheimer's disease phenotypes in model mice. *FASEB J* 27:174–186. [PubMed: 23038754]



32. Schnell E, Sizemore M, Karimzadegan S, Chen L, Brecht DS, Nicoll RA (2002): Direct interactions between PSD-95 and stargazin control synaptic AMPA receptor number. *Proc Natl Acad Sci U S A* 99:13902–13907. [PubMed: 12359873]
33. Dakoji S, Tomita S, Karimzadegan S, Nicoll RA, Brecht DS (2003): Interaction of transmembrane AMPA receptor regulatory proteins with multiple membrane associated guanylate kinases. *Neuropharmacology* 45:849–856. [PubMed: 14529722]
34. Delint-Ramirez I, Fernandez E, Bayes A, Kicsi E, Komiyama NH, Grant SG (2010): In vivo composition of NMDA receptor signaling complexes differs between membrane subdomains and is modulated by PSD-95 and PSD-93. *J Neurosci* 30:8162–8170. [PubMed: 20554866]
35. Chen X, Levy JM, Hou A, Winters C, Azzam R, Sousa AA, et al. (2015): PSD-95 family MAGUKs are essential for anchoring AMPA and NMDA receptor complexes at the postsynaptic density. *Proc Natl Acad Sci U S A* 112:E6983–6992. [PubMed: 26604311]
36. Kim E, Cho KO, Rothschild A, Sheng M (1996): Heteromultimerization and NMDA receptor-clustering activity of Chapsyn-110, a member of the PSD-95 family of proteins. *Neuron* 17:103–113. [PubMed: 8755482]
37. Niethammer M, Kim E, Sheng M (1996): Interaction between the C terminus of NMDA receptor subunits and multiple members of the PSD-95 family of membrane-associated guanylate kinases. *J Neurosci* 16:2157–2163. [PubMed: 8601796]
38. Banke TG, Bowie D, Lee H, Haganir RL, Schousboe A, Traynelis SF (2000): Control of GluR1 AMPA receptor function by cAMP-dependent protein kinase. *J Neurosci* 20:89–102. [PubMed: 10627585]
39. Ehlers MD (2000): Reinsertion or degradation of AMPA receptors determined by activity-dependent endocytic sorting. *Neuron* 28:511–525. [PubMed: 11144360]
40. Esteban JA, Shi SH, Wilson C, Nuriya M, Haganir RL, Malinow R (2003): PKA phosphorylation of AMPA receptor subunits controls synaptic trafficking underlying plasticity. *Nat Neurosci* 6:136–143. [PubMed: 12536214]
41. Sultana R, Banks WA, Butterfield DA (2010): Decreased levels of PSD95 and two associated proteins and increased levels of BCL2 and caspase 3 in hippocampus from subjects with amnesic mild cognitive impairment: Insights into their potential roles for loss of synapses and memory, accumulation of Aβ, and neurodegeneration in a prodromal stage of Alzheimer's disease. *J Neurosci Res* 88:469–477. [PubMed: 19774677]
42. Proctor DT, Coulson EJ, Dodd PR (2010): Reduction in post-synaptic scaffolding PSD-95 and SAP-102 protein levels in the Alzheimer inferior temporal cortex is correlated with disease pathology. *J Alzheimers Dis* 21:795–811. [PubMed: 20634587]
43. Gyllys KH, Fein JA, Yang F, Wiley DJ, Miller CA, Cole GM (2004): Synaptic changes in Alzheimer's disease: increased amyloid-beta and gliosis in surviving terminals is accompanied by decreased PSD-95 fluorescence. *Am J Pathol* 165:1809–1817. [PubMed: 15509549]
44. Roselli F, Tirard M, Lu J, Hutzler P, Lamberti P, Livrea P, et al. (2005): Soluble beta-amyloid1–40 induces NMDA-dependent degradation of postsynaptic density-95 at glutamatergic synapses. *J Neurosci* 25:11061–11070. [PubMed: 16319306]
45. Almeida CG, Tampellini D, Takahashi RH, Greengard P, Lin MT, Snyder EM, et al. (2005): Beta-amyloid accumulation in APP mutant neurons reduces PSD-95 and GluR1 in synapses. *Neurobiol Dis* 20:187–198. [PubMed: 16242627]
46. Leuba G, Savioz A, Vernay A, Carnal B, Kraftsik R, Tardif E, et al. (2008): Differential changes in synaptic proteins in the Alzheimer frontal cortex with marked increase in PSD-95 postsynaptic protein. *J Alzheimers Dis* 15:139–151. [PubMed: 18780974]
47. Leuba G, Walzer C, Vernay A, Carnal B, Kraftsik R, Piotton F, et al. (2008): Postsynaptic density protein PSD-95 expression in Alzheimer's disease and okadaic acid induced neuritic retraction. *Neurobiol Dis* 30:408–419. [PubMed: 18424056]
48. Bustos FJ, Ampuero E, Jury N, Aguilar R, Falahi F, Toledo J, et al. (2017): Epigenetic editing of the Dlg4/PSD95 gene improves cognition in aged and Alzheimer's disease mice. *Brain* 140:3252–3268. [PubMed: 29155979]



49. Yu L, Liu Y, Yang H, Zhu X, Cao X, Gao J, et al. (2017): PSD-93 Attenuates Amyloid-beta-Mediated Cognitive Dysfunction by Promoting the Catabolism of Amyloid-beta. *J Alzheimers Dis* 59:913–927. [PubMed: 28697571]
50. Krishnan ML, Van Steenwinckel J, Schang AL, Yan J, Arnadottir J, Le Charpentier T, et al. (2017): Integrative genomics of microglia implicates DLG4 (PSD95) in the white matter development of preterm infants. *Nat Commun* 8:428. [PubMed: 28874660]
51. Chuang CC, Jow GM, Lin HM, Weng YH, Hu JH, Peng YJ, et al. (2014): The punctate localization of rat Eag1 K+ channels is conferred by the proximal post-CNBHD region. *BMC Neurosci* 15:23. [PubMed: 24495567]
52. Tu S, Okamoto S, Lipton SA, Xu H (2014): Oligomeric A $\beta$ -induced synaptic dysfunction in Alzheimer's disease. *Mol Neurodegener* 9:48. [PubMed: 25394486]
53. Selkoe DJ, Hardy J (2016): The amyloid hypothesis of Alzheimer's disease at 25 years. *EMBO Mol Med* 8:595–608. [PubMed: 27025652]
54. Fourie C, Kim E, Waldvogel H, Wong JM, McGregor A, Faull RL, et al. (2014): Differential Changes in Postsynaptic Density Proteins in Postmortem Huntington's Disease and Parkinson's Disease Human Brains. *J Neurodegener Dis* 2014:938530. [PubMed: 26317010]
55. Murmu RP, Li W, Holtmaat A, Li JY (2013): Dendritic spine instability leads to progressive neocortical spine loss in a mouse model of Huntington's disease. *J Neurosci* 33:12997–13009. [PubMed: 23926255]
56. Stephens B, Mueller AJ, Shering AF, Hood SH, Taggart P, Arbuthnott GW, et al. (2005): Evidence of a breakdown of corticostriatal connections in Parkinson's disease. *Neuroscience* 132:741–754. [PubMed: 15837135]
57. Sunico CR, Dominguez G, Garcia-Verdugo JM, Osta R, Montero F, Moreno-Lopez B (2011): Reduction in the motoneuron inhibitory/excitatory synaptic ratio in an early-symptomatic mouse model of amyotrophic lateral sclerosis. *Brain Pathol* 21:1–15. [PubMed: 20653686]

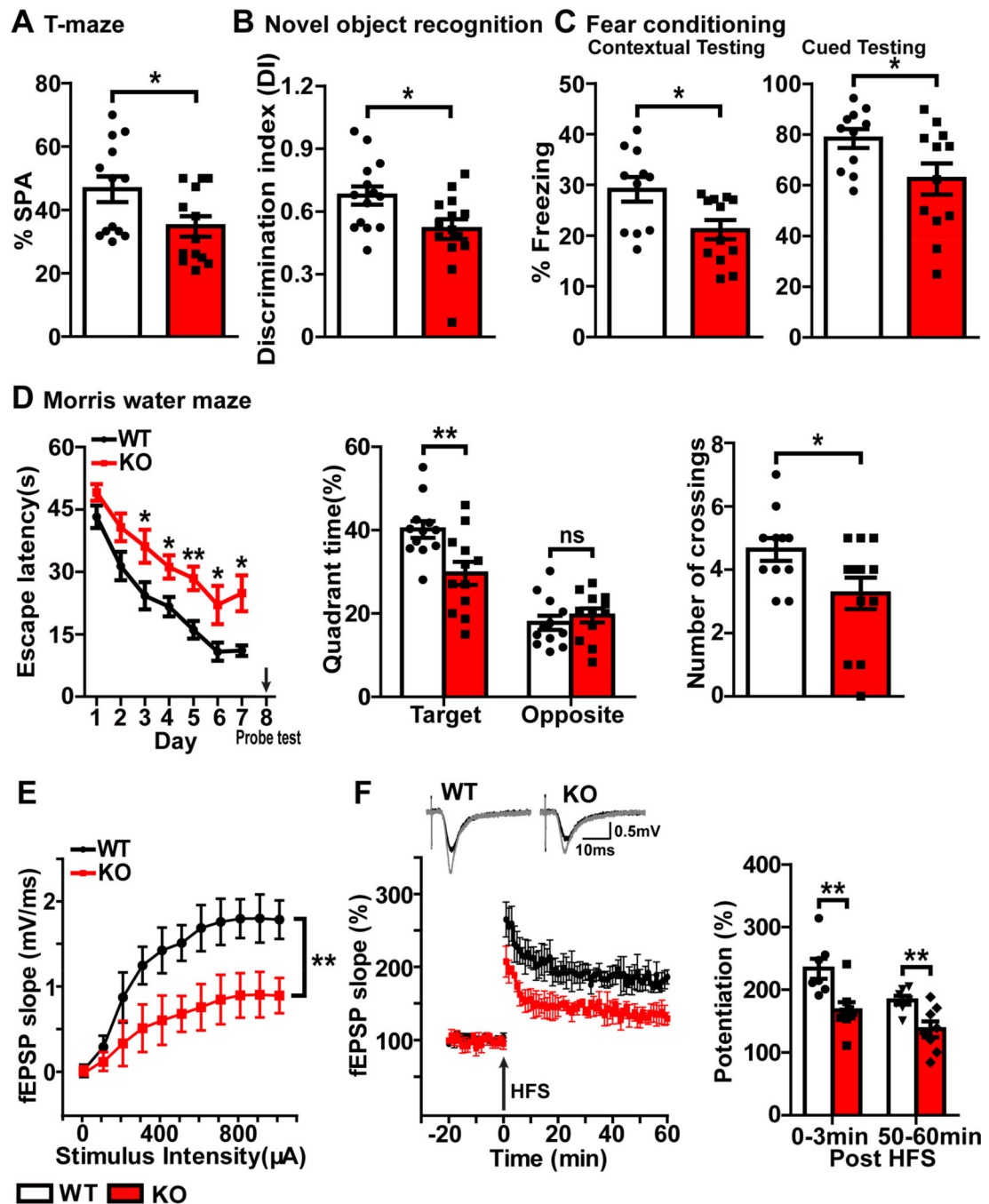


**Figure 1.**

*Rps23rg1* KO mice exhibit learning and memory deficits and synaptic plasticity impairment.

(A) *Rps23rg1* KO and wild type (WT) control mice were analyzed for spontaneous alternation (SPA) behavior by T-maze tests. Data represent mean  $\pm$  s.e.m. (KO,  $n = 13$ ; and WT,  $n = 13$ ).  $*P < 0.05$  (2-tailed Student's *t* test). (B) Mice were characterized using novel object recognition tests to determine their identification of a novel object (discrimination index). Data represent mean  $\pm$  s.e.m. (KO,  $n = 13$ ; and WT,  $n = 13$ ).  $*P < 0.05$  (2-tailed Student's *t* test). (C) In fear conditioning tests, mice were initially subjected to training and

their freezing response with contextual and cued fear stimuli was measured as a percentage of the testing duration. Data represent mean  $\pm$  s.e.m. (KO,  $n = 12$ ; and WT,  $n = 11$ ).  $*P < 0.05$  (2-tailed Student's  $t$  test). **(D)** Mice were analyzed for escape latency in Morris Water Maze tests within a 7-day training period. On the 8th day, mice were assayed for time spent in target and the opposite quadrants, in addition to the number of crossings over the platform region. Data represent mean  $\pm$  s.e.m. (KO,  $n = 12$ ; and WT,  $n = 12$ ). ns: not significant,  $*P < 0.05$ ,  $**P < 0.01$  (one way ANOVA test for escape latency comparison; 2-tailed Student's  $t$  test for others). **(E)** Input–output measurements from SC stimulation and subsequent recording in the CA1 stratum radiatum. Data represent mean  $\pm$  s.e.m. ( $n = 6$ –8 slices from 4–5 mice per group).  $**P < 0.01$  (repeated measures ANOVA). **(F)** LTP was induced by a two-train (100 Hz each) stimulus in the SC. Top panels depict representative fEPSP recording traces before and 60 min after high frequency stimulation (HFS, arrow). Mean fEPSP potentiation was determined from the fEPSP slopes calculated between 0–3 min and 50–60 min after HFS ( $n = 7$ –8 slices from 4–5 mice per group).  $**P < 0.01$  (2-tailed Student's  $t$  test).

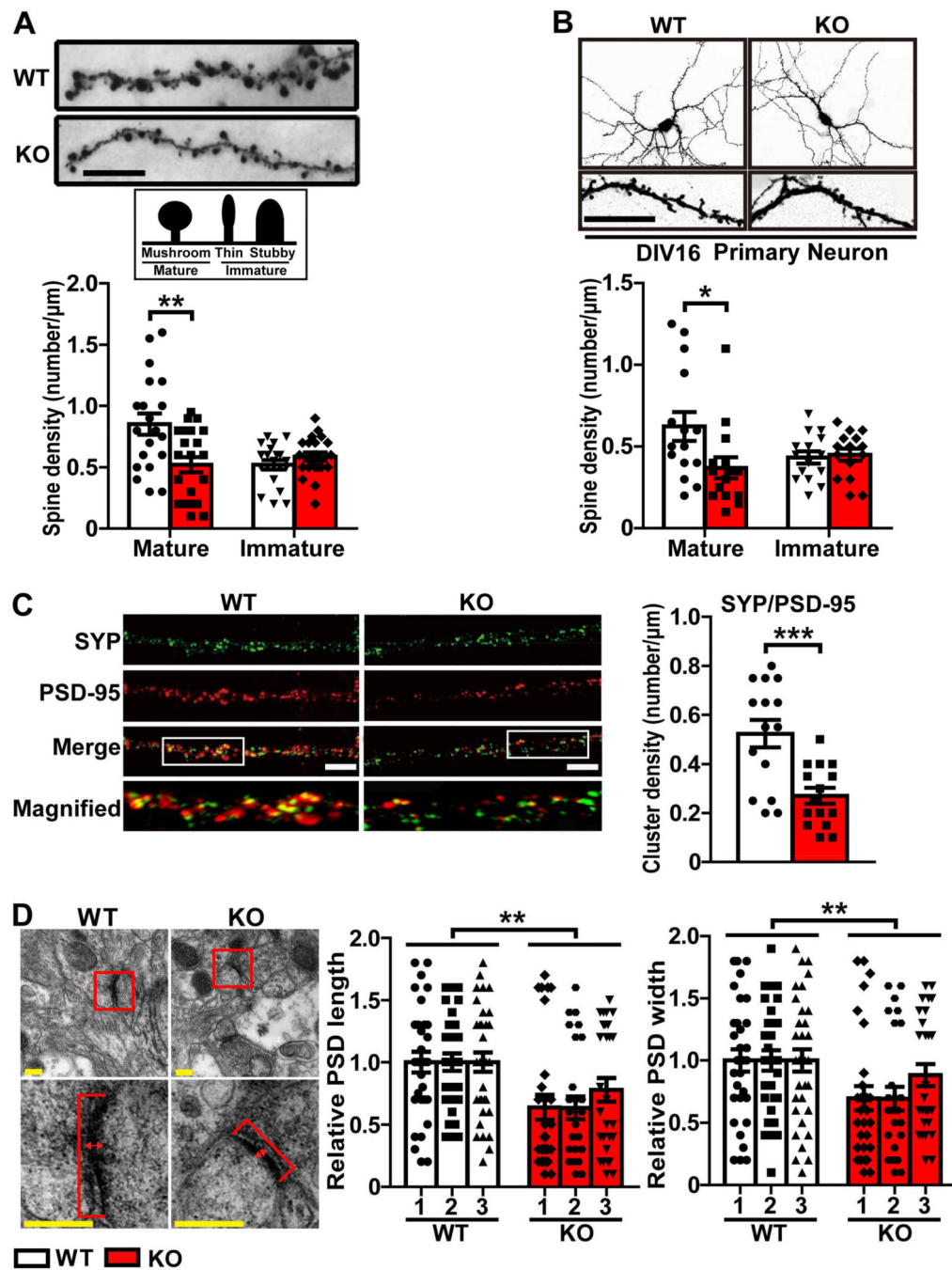


**Figure 2.** Impaired synapses in *Rps23rg1* KO mice. (A) The hippocampal CA1 region from 1-month-old WT and *Rps23rg1* KO mice was subjected to Golgi staining. Scale bars, 10  $\mu\text{m}$ . Mature (mushroom shape) and immature (thin and stubby shape) spines were quantified. Data represent mean  $\pm$  s.e.m.  $n = 20$ –22 neurons from 3 mice per group.  $**P < 0.01$  (2-tailed Student’s test). (B) Cultured primary neurons from WT and *Rps23rg1* KO mice were transfected with a pTomato plasmid at DIV7 and imaged by confocal microscope at DIV16. Scale bars: 10  $\mu\text{m}$ . Mature and immature spines were quantified. Data represent mean  $\pm$

s.e.m.  $n = 15$  neurons from 3 mice per group.  $*P < 0.05$  (2-tailed Student's test). **(C)** Cultured primary neurons from WT and *Rps23rg1* KO mice were immunostained for PSD-95 (in red) and synaptophysin (SYP, in green) and observed by confocal microscopy. Scale bars: 10  $\mu\text{m}$ . Numbers of PSD-95 and SYP co-clusters were quantified. Data represent mean  $\pm$  s.e.m.  $n = 15$  neurons from 3 mice per group.  $***P < 0.001$  (2-tailed Student's test). **(D)** Representative electron micrographic images of synapses in 1-month-old WT and *Rps23rg1* KO mouse hippocampus. Lower panels depict high-magnification images from regions indicated in the top panels, revealing individual synapses. Red bars and red arrows in lower panels indicate PSD length and PSD width, respectively. Scale bars, 200 nm. PSD length and width were quantified.  $n = 80\text{--}100$  synapses from 3 mice per group.  $**P < 0.01$  (2-tailed Student's test).

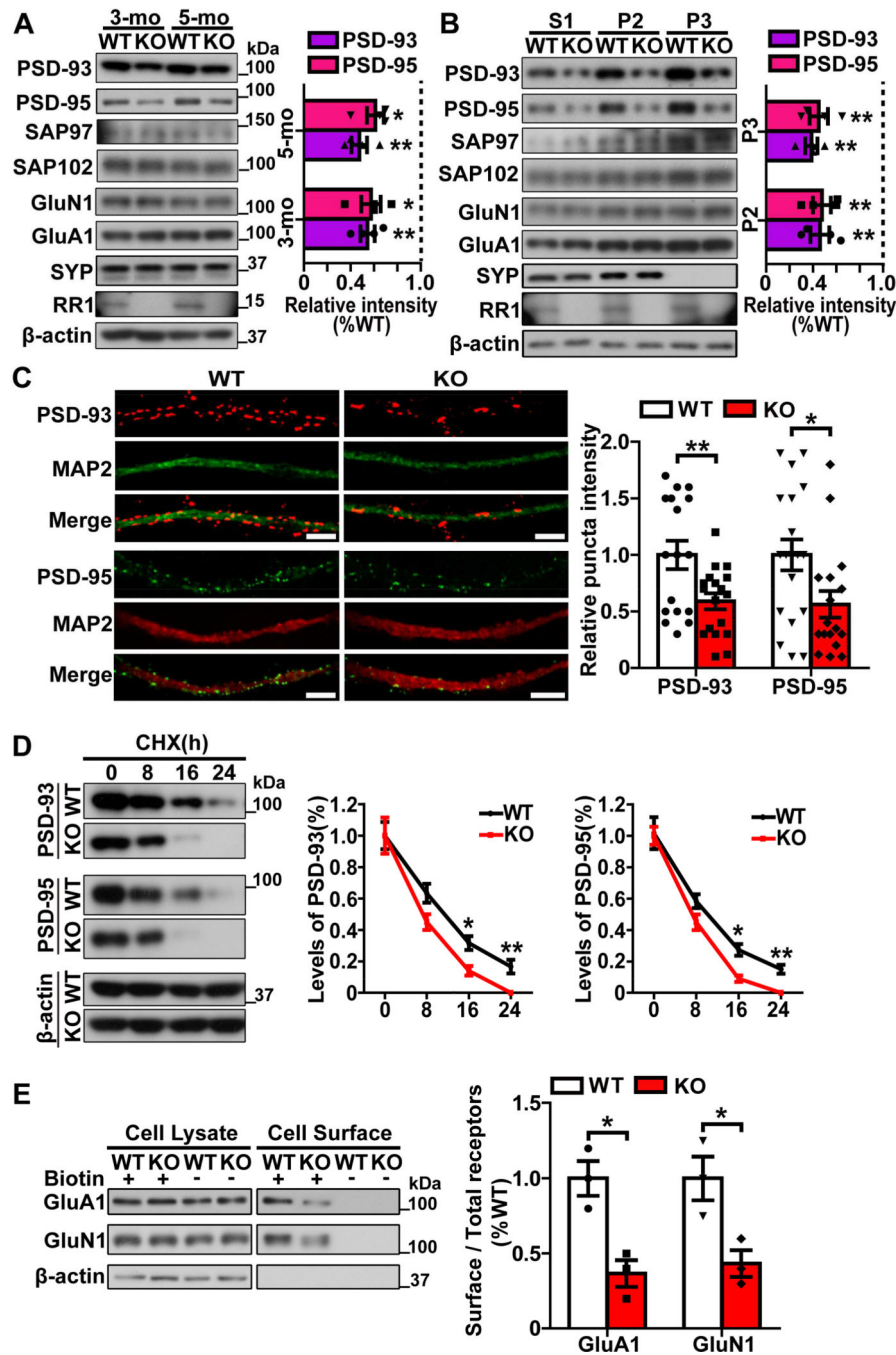


**Figure 3.** Loss of *Rps23rg1* enhances PSD-95 and PSD-93 turnover. (A,B) Equal protein quantities from total brain lysates derived from 3- and 5-month-old wild type (WT) and *Rps23rg1* KO mice (A), and total lysates (S1) and synaptosome fractions (P2 and P3) from 3-month-old WT and *Rps23rg1* KO mouse hippocampus (B) were subjected to immunoblotting for the proteins as indicated. PSD-93 and PSD-95 levels were quantified by densitometry and normalized to β-actin and compared to WT (set as to 1.0, dashed line). Data represent mean ± s.e.m. ( $n = 4$  mice per group). \* $P < 0.05$ , \*\* $P < 0.01$  (2-tailed Student's t test). (C)



Cultured primary neurons derived from WT and *Rps23rg1* KO mice were double-immunostained either for PSD-93 (in red) and MAP2 (in green) (upper panels), or for PSD-95 (in green) and MAP2 (in red) (lower panels). Immunofluorescence images were acquired by confocal microscopy. Scale bars, 10  $\mu$ m. PSD-93 clusters and PSD-95 clusters were quantified using ImageJ. Data represent mean  $\pm$  s.e.m.  $n = 17-19$  neurons from 3 mice per group.  $*P < 0.05$ ,  $**P < 0.01$  (2-tailed Student's t test). **(D)** Cultured primary neurons from wild type (WT) and *Rps23rg1* KO mice were treated with 30  $\mu$ M cycloheximide (CHX) for the time period indicated. PSD-93 and PSD-95 levels were examined by immunoblotting, quantified by densitometry, and normalized to  $\beta$ -actin (time 0 set to 1.0). Data represent mean  $\pm$  s.e.m. ( $n = 3$ ).  $*P < 0.05$ ,  $**P < 0.01$  (2-tailed Student's t test). **(E)** Cultured primary neurons from WT and *Rps23rg1* KO mice were subjected to cell surface biotinylation and immunoblotting. Biotinylated (cell surface) GluA1 and GluN1 levels were quantified by densitometry and normalized to total GluA1 and GluN1. Data represent mean  $\pm$  s.e.m. ( $n = 3$ ).  $*P < 0.05$  (2-tailed Student's t test).

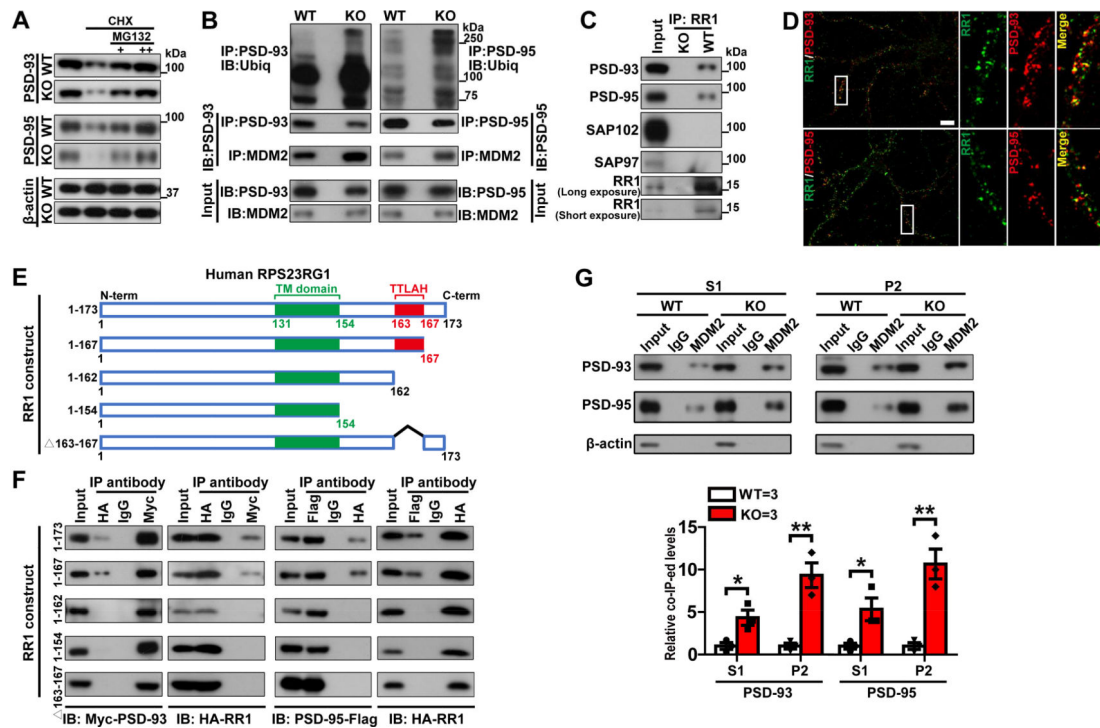


**Figure 4.**

RPS23RG1 interacts with PSD-93 and PSD-95, attenuating consequent ubiquitination by MDM2. (A) WT and *Rps23rg1* KO mouse primary neurons were treated with 30  $\mu$ M (cycloheximide) CHX in the presence of increasing MG132 (10 and 20  $\mu$ M) levels for 16 h. PSD-93 and PSD-95 levels were determined by immunoblotting. (B) Equal protein quantities from brain lysates generated from 3-month-old WT and *Rps23rg1* KO mice were subjected to immunoprecipitation (IP) with antibodies against MDM2 and PSD-93 (left panels) or PSD-95 (right panels). Precipitates were subjected to immunoblotting (IB) with antibodies against ubiquitin (Ubiq), and PSD-93 or PSD-95. Four percent of IP lysates were immunoblotted as input. (C) Equal protein quantities from brain lysates derived from 3-month-old WT and *Rps23rg1* KO mice were subjected to IP with an antibody against mouse RPS23RG1 (RR1), and immunoblotted with antibodies against the proteins as indicated. (D) HA-tagged human RR1 was transfected into WT mouse primary neurons at DIV4. Neurons were co-stained for hRR1 (in green) and PSD-93 (upper panels, in red) or PSD-95 (lower panels, in red) at DIV14, and imaged by confocal microscopy. High-magnification images of regions indicated are shown (right). Scale bars, 10  $\mu$ m. (E) Schematic depiction of human RPS23RG1 deletion constructs used: full-length RPS23RG1 (1–173), RPS23RG1 lacking the last 6 carboxyl-terminal amino acids (1–167), RPS23RG1 lacking the last 11 carboxyl-terminal amino acids (1–162), RPS23RG1 lacking the entire carboxyl-terminal intracellular region (1–154), and RPS23RG1 lacking the conserved “TTLAH” motif (163–167). (F) HEK 293T cells were co-transfected with Myc-PSD-93 or PSD-95-Flag, together with various human RPS23RG1 constructs tagged with HA. Cell lysates were subjected to IP with control IgG, and HA and Myc or Flag antibodies, and immunoblotted for the components as indicated. (G) Equal protein amounts of total lysates (S1) and synaptosome fractions (P2) from brain isolated from 3-month-old WT and *Rps23rg1* KO mice were

subjected to IP with IgG or an anti-MDM2 antibody, and immunoblotted with antibodies against PSD-93 and PSD-95. Immunoprecipitated PSD-93 and PSD-95 levels were quantified by densitometry and normalized to inputs (WT levels set to 1.0). Data represent mean  $\pm$  s.e.m. (n = 3). \* $P$  < 0.05, \*\* $P$  < 0.01 (2-tailed Student's t test).

Author Manuscript

Author Manuscript

Author Manuscript

Author Manuscript

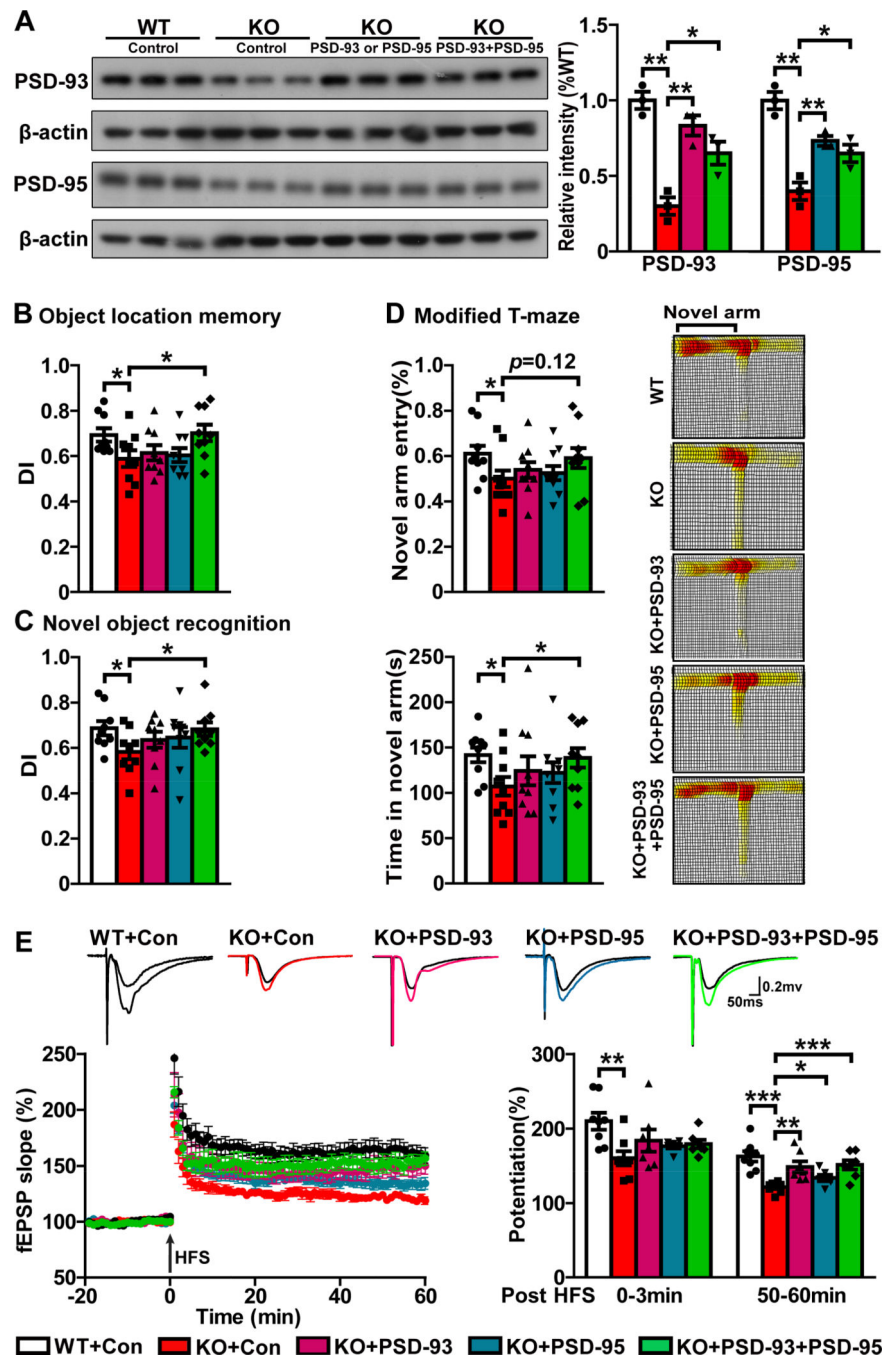


**Figure 5.** Restoration of PSD-93 and PSD-95 expression rescues memory and synaptic plasticity deficits in *Rps23rg1* KO mice. (A) WT and *Rps23rg1* KO mice at P0 were bilaterally co-injected with control adenovirus and control lentivirus, control adenovirus and lentivirus expressing PSD-93, control lentivirus and adenovirus expressing PSD-95, or lentivirus expressing PSD-93 and adenovirus expressing PSD-95. After behavioral and electrophysiological analyses, PSD-93 and PSD-95 protein levels from brain extracts were analyzed by immunoblotting and their levels were quantified by densitometry and

normalized to  $\beta$ -actin. Data represent mean  $\pm$ s.e.m. ( $n = 3$  mice per group).  $*P < 0.05$ ,  $**P < 0.01$  (2-tailed Student's test). **(B-D)** At 2 months of age, mice were subjected to behavioral analyses, where discrimination index (DI) in object location memory tests **(B)** and in object recognition memory tests **(C)**, and numbers of entries into and time spent in the novel arm in the modified T-maze test **(D)** were compared. Representative traces in the modified T-maze test are also shown. Data represent mean  $\pm$  s.e.m. ( $n = 9$  mice per group).  $*P < 0.05$  (2-tailed Student's test). **(E)** LTP was induced using a two-train (100 Hz each) stimulus in the SC. The top shows representative fEPSP recordings before and 60 min after high frequency stimulation (HFS, arrow). Mean fEPSP potentiation was quantified at 0–3 min and 50–60 min after HFS. Data represent mean  $\pm$ s.e.m. (WT+Con:  $n = 8$  slices from 4 mice; WT+Con:  $n = 8$  slices from 4 mice; KO+Con:  $n = 7$  slices from 5 mice; KO+PSD-93:  $n = 7$  slices from 4 mice; KO+PSD-95:  $n = 6$  slices from 4 mice; KO+PSD-93+PSD-95:  $n = 7$  slices from 4 mice).  $*P < 0.05$ ,  $**P < 0.01$ ,  $***P < 0.001$  (2-tailed Student's test).

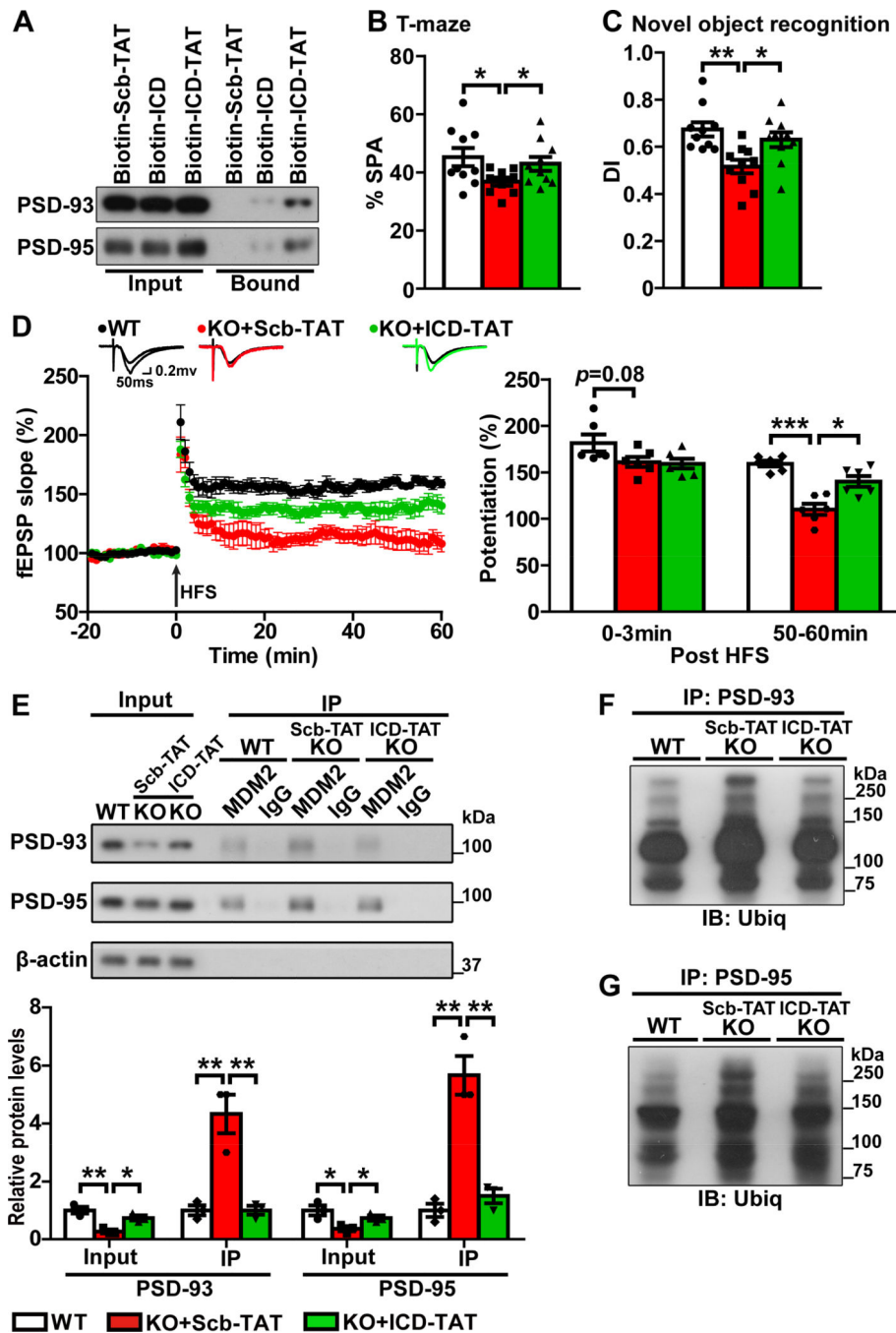


**Figure 6.** A RPS23RG1 intracellular domain-derived peptide rescues memory and synaptic plasticity deficits in *Rps23rg1* KO mice. (A) WT mice were subjected to 40 mg/kg/d i.p. injection of the peptides indicated. Mice were sacrificed 24 h after injection, and equal protein amounts from brain lysates were precipitated with avidin beads and immunoblotted with antibodies against PSD-93 and PSD-95. (B,C) WT mice were injected with a vehicle control and *Rps23rg1* KO mice were injected with FITC-conjugated ICD-Tat or Scb-Tat peptides (40 mg/kg/d, i.p.) for 3 consecutive days. Mice were then analyzed for spontaneous alternation



(SPA) in T-maze tests (**B**) and discrimination index (DI) was determined by novel object memory test (**C**). Data represent mean  $\pm$  s.e.m. ( $n = 10$  mice per group).  $*P < 0.05$ ,  $**P < 0.01$  (2-tailed Student's *t* test). (**D**) LTP was induced using a two-train (100 Hz each) stimulus in the SC. Representative fEPSP trace recordings before and 60 min after high frequency stimulation (HFS, arrow) are shown (top). Mean fEPSP potentiation was quantified at 0–3 min and 50–60 min after HFS. Data represent mean  $\pm$  s.e.m. ( $n = 6$  slices from 4 mice per group).  $*P < 0.05$ ,  $***P < 0.001$  (2-tailed Student's *t* test). (**E**) Equal protein quantities from brain lysates isolated from injected mice were subjected to immunoprecipitation (IP) with IgG or an anti-MDM2 antibodies, and immunoblotted with anti-PSD-93 and anti-PSD-95 antibodies. Four percent of the IP lysates were immunoblotted as input. Input PSD-93 and PSD-95 levels were quantified by densitometry and normalized to  $\beta$ -actin. Precipitated PSD-93 and PSD-95 levels were quantified by densitometry and normalized to respective input levels. Data represent mean  $\pm$  s.e.m. ( $n = 3$ ).  $*P < 0.05$ ,  $**P < 0.01$  (2-tailed Student's *t* test). (**F,G**) Equal protein quantities from brain lysates isolated from injected mice were subjected to IP with antibodies against PSD-93 (**F**) or PSD-95 (**G**), and then immunoblotted with an anti-ubiquitin (Ubiq) antibody.

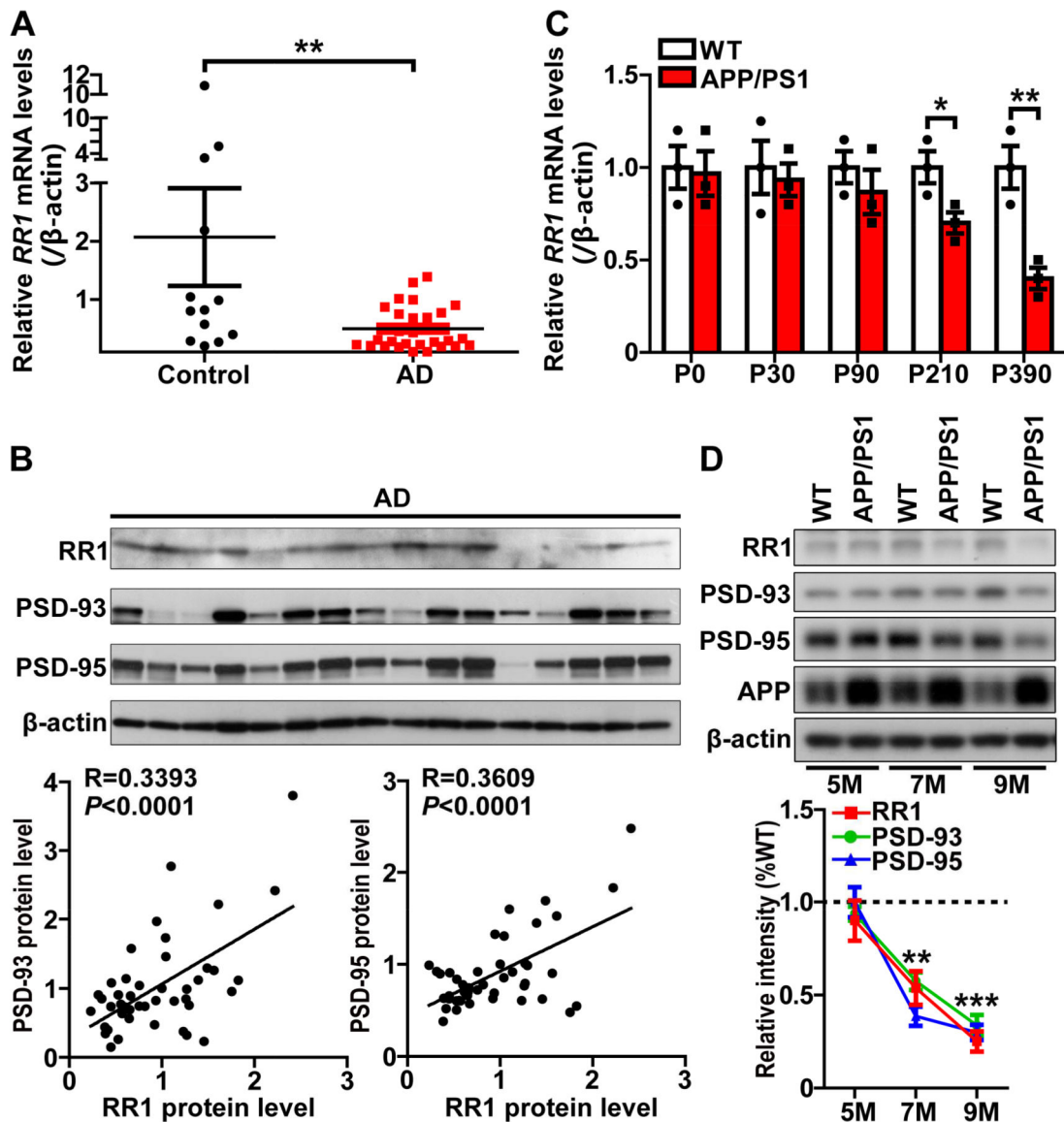


**Figure 7.**

*RPS23RG1* levels are reduced in human and mouse AD brain, and correlates with PSD-95 and PSD-93 levels. **(A)** Human *RPS23RG1* (*RR1*) mRNA levels from AD patient and control brain were determined by quantitative real-time PCR (qRT-PCR) and normalized to 18s rRNA. Data represent mean ± s.e.m. (Controls: *n* = 13; and AD patients: *n* = 29). \*\**P* < 0.01 (2-tailed Student's *t*-test). **(B)** Human *RPS23RG1* (*RR1*), PSD-93, PSD-95 and β-actin protein levels in AD patient brain were analyzed by immunoblotting and quantified by densitometry. Protein quantities were normalized to β-actin, and correlations between human *RR1* and PSD-93 or PSD-95 were determined by regression analysis (*n* = 47). **(C)** *Rps23rg1* (*RR1*) mRNA levels in APP/PS1 and WT littermate mouse brain at different ages were quantified by qRT-PCR and normalized to β-actin. Data represent mean ± s.e.m. (*n* = 3 per group). \**P* < 0.05, \*\**P* < 0.01 (2-tailed Student's *t*-test). **(D)** Synaptosome fractions derived from WT and APP/PS1 mouse hippocampus at 5, 7 and 9 months of age were

subjected to immunoblotting for the proteins indicated. Protein levels of mouse RR1, PSD-93 and PSD-95 were quantified by densitometry, normalized to  $\beta$ -actin (levels at 5 months were set to 1.0). Data represent mean  $\pm$  s.e.m. ( $n = 4$  per age). \*\* $P < 0.01$ , \*\*\* $P < 0.001$  (2-tailed Student's t-test).

Author Manuscript

Author Manuscript

Author Manuscript

Author Manuscript

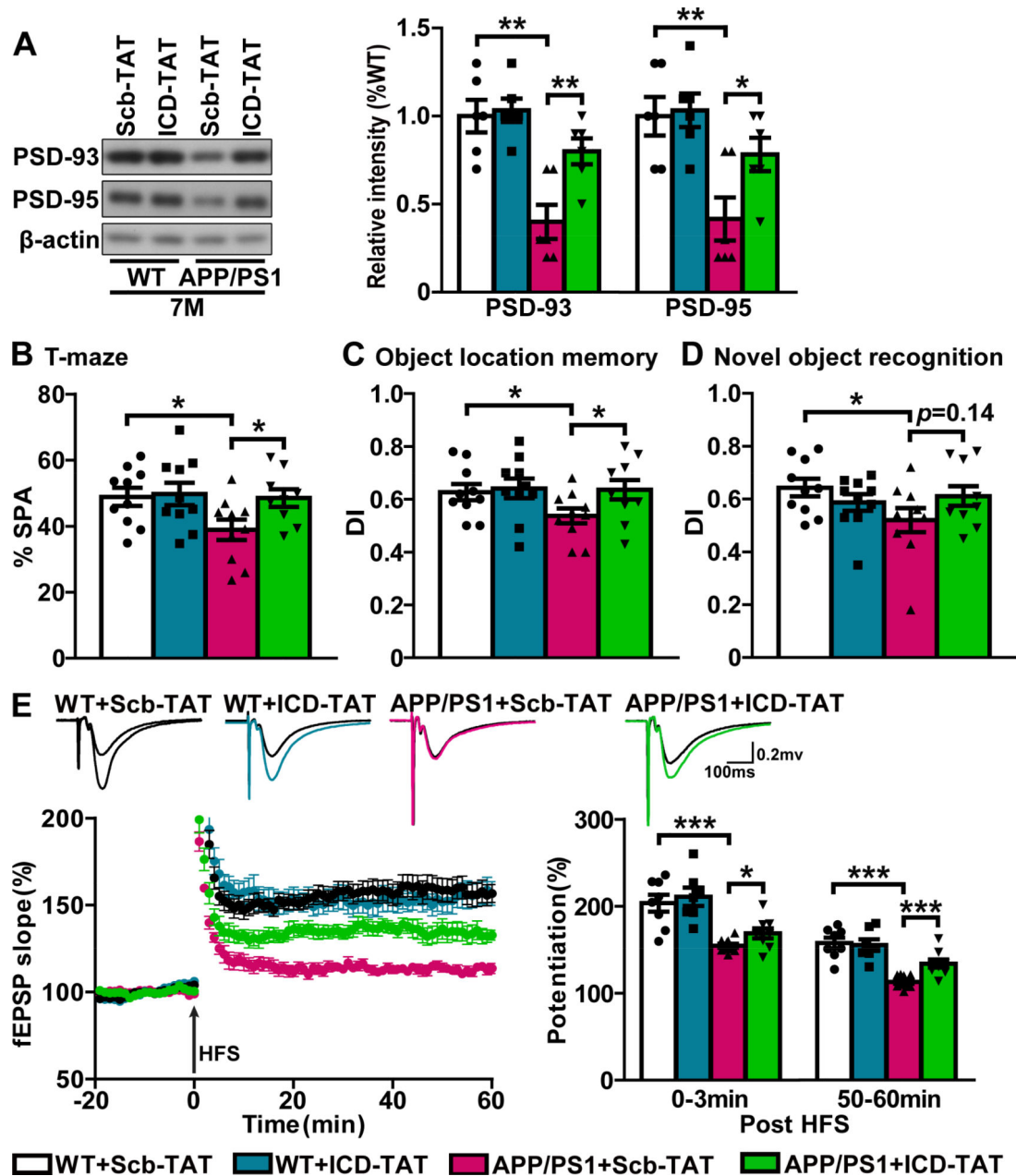


**Figure 8.**

A RPS23RG1 intracellular domain-derived peptide rescues memory and synaptic plasticity deficits in APP/PS1 AD model mice. (A) 7-month-old WT and APP/PS1 mice were subjected to FITC-conjugated ICD-Tat or Scb-Tat peptide injection (40 mg/kg/d, i.p. injection) for 3 consecutive days. Eight days later, mice were sacrificed and hippocampal synaptosome fractions were subjected to immunoblotting for the proteins indicated. PSD-93 and PSD-95 protein levels were quantified by densitometry and normalized to  $\beta$ -actin. Data represent mean  $\pm$  s.e.m. ( $n = 6$  per group). \* $P < 0.05$ , \*\* $P < 0.01$  (2-tailed Student's  $t$ -test). (B-D) Injected mice were subjected to behavioral analysis. Spontaneous alternation (SPA) in T-maze tests (B), and discrimination index (DI) in object location memory (C) and in novel

object recognition memory tests (**D**) were quantified. Data represent mean  $\pm$  s.e.m. ( $n = 9$  for APP/PS1+ICD-TAT group and  $n = 10$  for other groups).  $*P < 0.05$  (2-tailed Student's t-test). (**E**) LTP was induced using a two-train (100 Hz each) stimulus in the SC. Representative fEPSP trace recordings of responses before and 60 min after high frequency stimulation (HFS, arrow) are shown (top). Mean fEPSP potentiation was determined at 0–3 min and 50–60 min after HFS. (WT+Scb-TAT:  $n = 8$  slices from 5 mice; WT+ICD-TAT:  $n = 7$  slices from 5 mice; APP/PS1+Scb-TAT:  $n = 10$  slices from 5 mice; APP/PS1+ICD-TAT:  $n = 9$  slices from 5 mice).  $*P < 0.05$ ,  $***P < 0.001$  (2-tailed Student's t-test).